AIAA Atmospheric Flight Mechanics Conference
08 - 11 August 2011, Portland, Oregon

AIAA 2011-6640

Rapid Simultaneous Hypersonic Aerodynamic and Trajectory Optimization Using Variational Methods

Michael J. Grant*, Ian G. Clark†, and Robert D. Braun‡
Georgia Institute of Technology, Atlanta, GA, 30332

Traditional multidisciplinary design optimization methodologies of hypersonic missions often employ population-based global searching methods that rely on shooting methods to perform trajectory optimization. In this investigation, a rapid simultaneous hypersonic aerodynamic and trajectory optimization methodology is constructed based on variational methods. This methodology is constructed from two enabling advancements in analytic hypersonic aerodynamics and rapid trajectory optimization. Comparisons made with a single and multi-objective particle swarm optimizer highlight the computational advantages and improved solutions obtained through continuation of variational methods. The incorporation of trajectory constraints into the particle swarm optimization process through penalty functions or as additional objectives is shown to greatly increase the complexity of the design process. Alternatively, variational methods are able to precisely satisfy trajectory constraints without this added complexity. Examples demonstrate that Pareto frontiers in both vehicle and trajectory objectives can be constructed using variational methods. For convex frontiers, this is performed using a weighted sum of the objectives. For non-convex frontiers, the optimization is performed through continuation of a set of constrained objectives.

Nomenclature

APAS	Aerodynamic Preliminary Analysis System
CFD	Computational Fluid Dynamics
CBAERO	Configuration Based Aerodynamics
DSM	Design Structure Matrix
HABP	Hypersonic Arbitrary Body Program
MDO	Multidisciplinary Design Optimization
PSO	Particle Swarm Optimizer
MOPSO	Multi-Objective Particle Swarm Optimizer

A	vehicle reference area, m^2	L/D	lift to drag ratio
C_D	drag coefficient	m	vehicle mass, kg
C_L	lift coefficient	n	number of objectives
D	drag force magnitude, N	$\dot{q}$	heat rate, W/cm^2
d	vehicle half angle, rad	r	radial magnitude, m
H	scale height, m	r_e	Earth radius, m
I	path cost	t	time, s
J	cost functional	t_0	initial time, s
J'	augmented objective	t_f	final time, s
L	lift force magnitude, N	$\mathbf{u}$	control vector

*Graduate Research Assistant, Guggenheim School of Aerospace Engineering, AIAA Student Member.
†Visiting Assistant Professor, Guggenheim School of Aerospace Engineering, AIAA Member.
‡David and Andrew Lewis Associate Professor of Space Technology, Guggenheim School of Aerospace Engineering, AIAA Fellow.

v	relative velocity magnitude, m/s	θ	downrange subtended angle, rad
$\mathbf{x}$	state vector	ρ_0	atmospheric density at the surface, kg/m^3
α	angle of attack, deg	Φ	terminal cost
γ	relative flight path angle, rad	ϕ	bank angle, deg
λ	costate		
μ	gravitational parameter, m^3/s^2		

I. Introduction

Traditionally, conceptual design is performed using various tools provided by disciplinary experts. The interaction among the resulting contributing analyses during hypersonic mission design is often illustrated using a design structure matrix (DSM) as shown in Figure 1. In this methodology, design variables are often chosen within each discipline, and a multidisciplinary design optimization (MDO) scheme is used to optimize the overall system.[1–7] Due to the challenges associated with simultaneously accounting for all major disciplines, MDO algorithms operate on the various connections among the contributing analyses in an efficient manner. In this approach, a direct optimization methodology is often used to optimize this finite set of design variables. As a result, continuous design variables such as trajectory paths must be discretized for incorporation into these methods. In general, these MDO methods assume that each contributing analysis is provided to the designer in which little or no modification can be made (*e.g.*, legacy codes).

While these traditional advances in MDO are important for conceptual design, they neglect advancements that can be made within the individual contributing analyses to improve the overall design process. While traditional MDO methodologies enable system level metrics such as cost and risk to be included in the system design process, designers of high performance hypersonic missions are initially interested in the extent of vehicle performance that can be achieved. If this envelope of vehicle performance includes missions of interest, then trades in system level metrics can follow. To address high performance entry missions, advances have been made to hypersonic aerodynamic modeling and trajectory optimization.[8,9] Specifically, the construction of analytic hypersonic aerodynamic relations and a rapid trajectory optimization framework based on continuation of variational methods enables the construction of a unified mathematical framework to perform rapid simultaneous hypersonic aerodynamic and trajectory optimization for conceptual design.

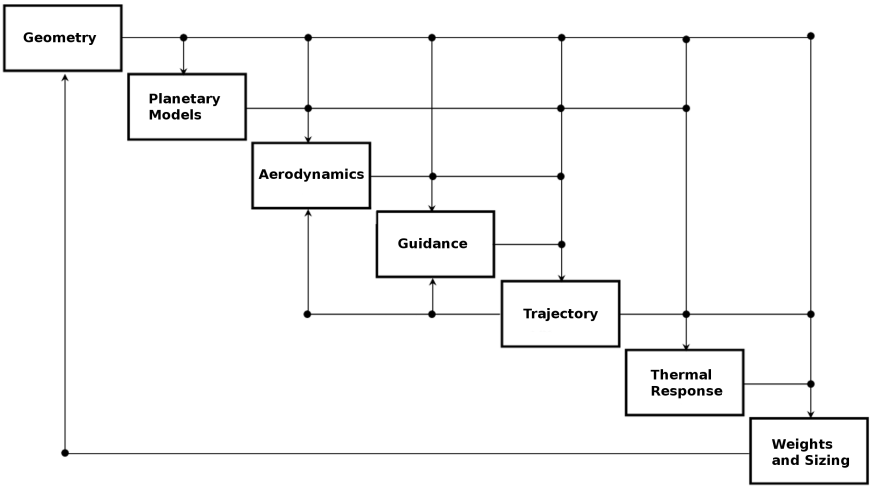

Figure 1. Example design structure matrix for entry systems.[10]

II. Enabling Advancements

II.A. Analytic Hypersonic Aerodynamics

Traditionally, the hypersonic aerodynamics of a vehicle is characterized from computational fluid dynamics (CFD). Due to the substantial computational requirements of CFD, vehicles are generally chosen that provide the necessary aerodynamic performance, such as L/D and ballistic coefficient, to accomplish a given mission.

Subsequently, the vehicle is designed to meet these performance constraints. During conceptual design, methods are typically employed to improve computational speed at the expense of a small reduction in fidelity. For example, panel methods derived from Newtonian flow theory can be used to obtain the hypersonic aerodynamics of a vehicle with only a fraction of the computational requirements of CFD.[11] Although panel methods are much faster than CFD, the designer is still required to limit the number of vehicle shapes analyzed due to the relatively high remaining computational requirements of evaluating other disciplines within traditional MDO frameworks. Consequently, a vehicle shape is usually chosen prior to trajectory design. Once the trajectory has been designed for the given vehicle, an iterative MDO process is performed to alter the vehicle dimensions until the proper hypersonic aerodynamics is found to accomplish the desired mission.

Panel methods, including those within the Hypersonic Arbitrary Body Program (HABP) in conjunction with the Aerodynamic Preliminary Analysis System (APAS) and the Configuration Based Aerodynamics Tool (CBAERO), have been widely used during conceptual design due to the ability of these methods to rapidly evaluate the hypersonic aerodynamics of complex, arbitrary shapes.[12–15] These tools construct large aerodynamic tables that must be interrogated at the various angles of attack and sideslip flown throughout the trajectory. However, many analytic vehicle configurations have been used for previous missions, and many of these same configurations are currently studied to accomplish future missions. For example, many robotic entry systems at Earth and Mars have consisted of a sphere-cone forebody. Additionally, crewed vehicles such as the Apollo command module and planned Orion capsule utilize a spherical forebody. Finally, many high performing missions to support hypersonic military applications and human exploration of Mars have employed blunted biconics and triconics. The geometry of these vehicles can be expressed analytically, and as a result, the corresponding hypersonic aerodynamics of these vehicles can also be expressed analytically for various angles of attack and sideslip.[8] The analytic hypersonic aerodynamic relations enable vehicle shape parameters to be analytically incorporated into the trajectory equations of motion. As a result, the large aerodynamic tables that contribute to the segregated, iterative process of traditional MDO methods are eliminated. This enables the simultaneous hypersonic aerodynamic and trajectory optimization problem to be expressed in an analytical form that allows recent advances in rapid trajectory optimization to be extended to also include vehicle shape.

II.B. Rapid Trajectory Optimization Using Variational Methods

In many trajectory optimization algorithms, the aerodynamics of the vehicle is assumed to be specified *a priori*. As a result, many trajectory optimization methodologies have been developed with the intent of identifying a single optimal trajectory for a given mission and vehicle shape. However, during conceptual design, many optimal trajectories must be constructed efficiently. Prior work has shown that rapid design space exploration of optimal trajectories can be accomplished using only the continuation of fast variational (indirect) methods.[16–20] Additionally, prior work has shown that this process is effective for a wide range of vehicle shapes, constraints, environment parameters, initial conditions, and terminal conditions.[9] This has eliminated the need to balance the large region of attraction associated with direct methods with the computational efficiency of indirect methods as depicted in Table 1.

Table 1. Comparison between direct and variational methods.

	Advantages	*Disadvantages*
Direct Methods	Large region of attraction	Computationally intensive
	Widespread NLP solvers exist	Optimality not guaranteed
Variational (Indirect) Methods	Rapid convergence	Small region of attraction
	Necessary conditions satisfied	Costates introduced

The use of variational methods over slower direct methods is enabled by the analytic formulation of the trajectory optimization problem shown in Eq. (1), where J is the cost functional that is minimized, Φ is the terminal cost, and $\int_{t_0}^{t_f} Idt$ is the path cost. Terminal constraints are present for many hypersonic missions and are expressed in the form of Eq. (2). Finally, the equations of motion are given in the form of Eq. (3).

$$J = \Phi[\mathbf{x}(t_f), t_f] + \int_{t_0}^{t_f} I(\mathbf{x}(t), \mathbf{u}(t), t)dt \tag{1}$$

$$\Psi[\mathbf{x}(t_f), t_f] = 0 \tag{2}$$

$$\dot{\mathbf{x}} = f[\mathbf{x}(t), \mathbf{u}(t), t], \quad t_0 \text{ given} \tag{3}$$

For this study, a planar entry trajectory is assumed with equations of motion shown in Eq. (4)-(7), where r is the radial magnitude, θ is the downrange subtended angle, v is the relative velocity magnitude, γ is the relative flight path angle, D is the drag force magnitude, m is the mass of the vehicle, μ is the gravitational parameter, L is the lift force magnitude, and ϕ is the bank angle. By including the analytic aerodynamic relations into these equations of motion, the analytic trajectory optimization problem can be extended into a simultaneous analytic vehicle and trajectory optimization problem, enabling rapid multidisciplinary optimization using variational methods.

$$\dot{r} = v \sin\gamma \tag{4}$$

$$\dot{\theta} = \frac{v\cos\gamma}{r} \tag{5}$$

$$\dot{v} = -\frac{D}{m} - \frac{\mu \sin\gamma}{r^2} \tag{6}$$

$$\dot{\gamma} = \frac{L\cos\phi}{mv} + \left(\frac{v}{r} - \frac{\mu}{vr^2}\right)\cos\gamma \tag{7}$$

III. Multidisciplinary Optimization Comparison Methodologies

III.A. Variational Methods

III.A.1. Augmentation of the Rapid Trajectory Optimization Methodology

To optimize the vehicle simultaneously with the trajectory, the equations of motion shown in Eq. (4)-(7) must be augmented with the appropriate analytic aerodynamic relations.[8] For example, the analytic aerodynamics of a conical frustum can be parametrized by the cone half angle, d. As a result, the aerodynamic forces in Eq. (6) and (7) can be expressed as a function of vehicle shape as shown in Eq. (8) and (9). As new shape parameters such as the cone half angle are introduced into the equations of motion, a new state can be added as shown in Eq. (10). For this study, shape parameters are assumed to be constant throughout the trajectory. If the shape of the vehicle can be altered during flight, for example to control inflatable aerodynamic decelerators during entry, then Eq. (10) can be modified accordingly. When applying variational methods to this augmented system, a costate is introduced for each corresponding shape parameter. If the objective is only a function of the trajectory in the form of Eq. (1), then the indirect method can be extended to include the additional states and costates associated with each shape parameter. As a result, optimal solutions in both vehicle and trajectory are simultaneously constructed. In this work, the BVP4C function within Matlab is used to solve for the variational solutions. Note that variational methods can only perform a single objective optimization expressed through the cost functional, J. If vehicle objectives are also included, then the optimization must be modified according to the convexity of the Pareto frontier.

$$\dot{v} = -\frac{D(d)}{m} - \frac{\mu \sin\gamma}{r^2} \tag{8}$$

$$\dot{\gamma} = \frac{L(d)\cos\phi}{mv} + \left(\frac{v}{r} - \frac{\mu}{vr^2}\right)\cos\gamma \tag{9}$$

$$\dot{d} = 0 \tag{10}$$

III.A.2. Multi-Objective Formulation

If the Pareto frontier is convex, then an augmented objective, J', can be constructed through the combination of multiple objectives as shown in Eq. (11) for n objectives. The influence of each individual objective, J_i, can be controlled through the corresponding relative weighting, w_i. The Pareto frontier can be constructed by performing successive optimizations through continuation of these weightings. This approach minimizes the added complexity required to perform a multiobjective optimization but has been shown to be ineffective for non-convex frontiers.[21–23] Various approaches have been developed to address non-convex frontiers, including transformations to convex shapes and the addition of constraints. For this work, non-convex frontiers are addressed by performing a single objective optimization in J_i while constraining the remaining objectives to specific values. The Pareto frontier is then constructed through continuation of the constrained objective values. It is important to note that this approach will also work for convex Pareto frontiers. However, the added complexity that results from the addition of constraints can reduce the efficiency of the continuation process for convex frontiers. In general, the convexity of the Pareto frontier will not be known *a priori*. As such, an augmented objective can be used to identify the convex portions of the frontier. If any gaps are observed in the Pareto frontier, then the continuation of constrained objectives can be used to identify these non-convex regions.

$$J' = \frac{1}{\sum_{i=0}^{n} w_i} \cdot \sum_{i=0}^{n} w_i J_i \tag{11}$$

III.B. Baseline Multidisciplinary Optimization Methodology

To illustrate the advantages of variational methods for design, comparisons are made to a baseline multidisciplinary optimization methodology. While numerous MDO algorithms and techniques exist, many recent entry design studies have used population-based global searching algorithms such as genetic algorithms and particle swarm optimizers.[6,7,24,25] As such, a particle swarm optimizer (PSO) was chosen to perform these comparisons. Parameters associated with the PSO were chosen based on prior experience.[24] Note that the choice in these parameters can dramatically influence the efficiency of the optimization process, but identifying an optimal set of parameters *a priori* is not practical.[26] Due to the stochastic nature of the algorithm, a sufficient number of iterations was chosen based on available computational resources or when marginal improvement of the optimal solution was observed. In general, the optimizer required a population size of 100 particles that searched the design space for approximately 300 iterations.

The PSO solves for optimal solutions through direct shooting of the equations of motion shown in Eq. (4)-(7) in which free initial states, a discretized bank profile, and vehicle parameters form the design space.[24,25] In this study, ten discrete bank angles are chosen at equidistant velocity increments throughout the entry, and the bank angle at any point along the trajectory is calculated by linear interpolation of these angles. The trajectory is propagated from the initial state until the vehicle reaches either the desired terminal velocity or the ground at 0 km altitude. Although many traditional MDO methods employ panel methods to characterize the hypersonic aerodynamics of a vehicle, the analytic aerodynamics were used as a substitute to make reasonable comparisons with variational methods. To highlight some of the challenges associated with using traditional MDO methods to perform simultaneous hypersonic aerodynamic and trajectory optimization, comparisons are made to solutions obtained from variational methods.

IV. Comparison of Variational Methods and Baseline Multidisciplinary Optimization Methodology

For the following comparisons, an Earth-based entry is chosen with environment parameters shown in Table 2. An exponential atmosphere and a spherical mass distribution of the Earth are assumed. To improve execution speed by approximately a factor of 30, the required functions to solve for the variational solutions and perform trajectory propagations for the PSO are autocoded into C from Matlab. In all comparisons, the initial and terminal conditions in altitude and velocity are assumed to be fixed, whereas the initial and terminal conditions in flight path angle and downrange are assumed to be free. To highlight a range of shapes that can be included in the optimization, the following examples consist of a blunted cone, blended wedge, and blunted biconic. The mass for each vehicle was chosen to provide a reasonable ballistic coefficient to provide a wide range of solutions. As such, entry masses of 4100 kg for the blunted cone, 16,300 kg for the blended wedge, and 410 kg for the blunted biconic were chosen. For each vehicle, the mass is assumed to be constant throughout the flight. As a result, the ballistic coefficient of each vehicle is varied as the shape is modified during the optimization process. Finally, the angle of attack of the blunted cone and blended wedge was chosen to be 20^o, and the angle of attack of the blunted biconic was chosen to be 10^o.

Table 2. Environment parameters.

Parameter	*Value*
Scale Height, H	7200 m
Surface Density, ρ_o	1.217 kg/m^3
Gravitational Parameter, μ	3.986e14 m^3/s^2
Earth Radius, r_e	6378000 m

IV.A. Minimum Heat Load for a Blunted Cone Subject to Terminal Constraints

As an initial comparison of the two methodologies, the trajectory and geometry of a blunted cone are simultaneously optimized to minimize stagnation point heat load resulting from minor blunting of the nose. This trajectory objective was chosen to enable comparisons with examples from prior work.[9,20] To minimize heat load, the heat rate must be maximized along every portion of the trajectory, and this result is evident from the optimal solutions presented in this report. Additionally, this prior work has shown that unconstrained optimal trajectories can be quickly constructed through continuation of variational solutions from a short, unconstrained trajectory that is relatively easy to optimize.[9] This approach is repeated on the augmented system in which the vehicle is also optimized during the continuation process. During the optimization, the analytic aerodynamics of the blunted cone is altered through modification of the cone half angle, d. In this work, the short, unconstrained trajectory is chosen to have the desired terminal conditions in altitude and velocity. As such, a continuation is chosen to modify the initial conditions in altitude and velocity to match the desired entry conditions. During this process, the initial velocity is originally increased while maintaining a fixed initial altitude. After this continuation in initial velocity, the initial altitude is increased to match the desired initial conditions as shown in Figure 2. Additionally, Figure 3 shows the evolution of the corresponding costates. During this series of optimizations, the initial and terminal conditions in flight path angle and downrange are allowed to vary. As expected, λ_γ and λ_θ are zero at the initial and terminal points of the trajectory. Furthermore, λ_θ is identically zero throughout the trajectory as expected by the absence of θ in the equations of motion shown in Eq. (4)-(7).

During the continuation process, the cone half angle, d, is also optimized to provide minimum heat load trajectories. As expected, each solution consists of an optimal cone angle of 90^o. This forms the most blunt conic vehicle in the shape of a circular disk. This shape minimizes heat load by minimizing the ballistic coefficient of the vehicle, and, consequently, the flight time of the trajectory. Additionally, the flight path angle costate is negative throughout the trajectory, resulting in a constant commanded bank angle of 180^o as expected to fly full lift-up for a blunt body as described by the switching structure shown in Table 3. This allows the vehicle to fly a steep entry that further reduces flight time. These expected minimum heat load solutions that are consistent with prior studies validate the simultaneous hypersonic aerodynamic and trajectory optimization framework.[9,20]

Table 3. Control switching structure.

$C_L \cdot \lambda_\gamma < 0$	Bank = 0 deg
$C_L \cdot \lambda_\gamma > 0$	Bank = 180 deg
$C_L \cdot \lambda_\gamma = 0$	Bank is indeterminate

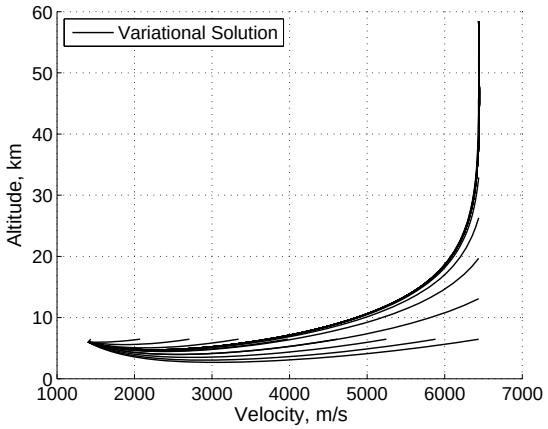

Figure 2. Continuation of minimum heat load solutions.

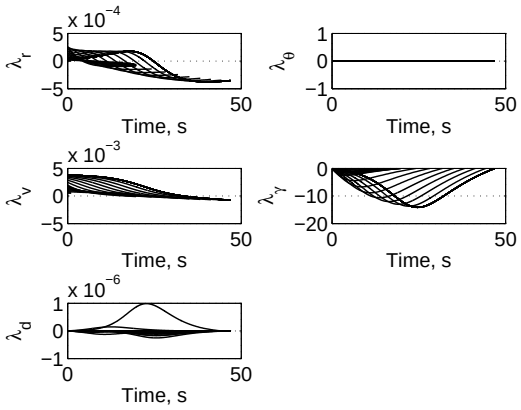

Figure 3. Corresponding minimum heat load costates.

For comparison, a single objective PSO is also used to perform the same hypersonic aerodynamic and trajectory optimization from the desired initial conditions. Variational methods convert the optimization problem into a root-solving problem, and, as a result, trajectory constraints are easily enforced along the optimal solution. Alternatively, trajectory constraints are indirectly enforced by the PSO through modification of the bank angle profile. As a result, penalty functions are generally constructed to enforce trajectory constraints. The optimization is then performed on the augmented objective function that includes these penalty functions rather than the original objective function of interest. After selection of the penalty function, the designer must choose an appropriate balance between the original objective and this penalty when constructing the augmented objective function.

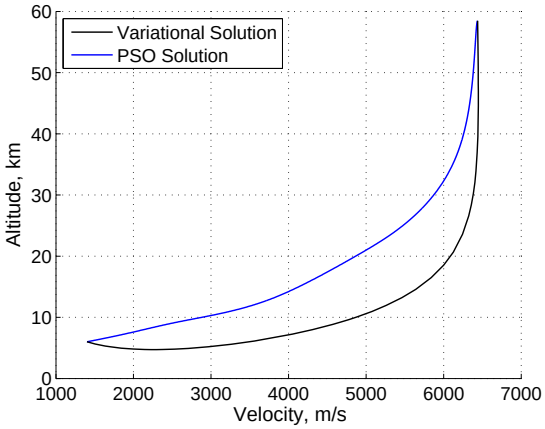

Figure 4. Comparison between variational method and PSO with strong terminal conditions penalty.

If the penalty associated with the terminal constraint is too strong, then the trajectory will be optimized to the constraint. As a result, the trajectory objective will be largely ignored as shown in Figure 4 in which the heat load is multiplied by the magnitude of the final altitude error. While the optimal PSO solution consists of a cone half angle of 89.3^o, the heat load is 2.26 times greater than that of the variational solution. To construct minimum heat load solutions, the penalty must be relaxed. This can be done by constructing a sphere around the terminal constraints in which any terminal points inside this sphere are not penalized, and any points outside of this sphere are strongly penalized in the same manner as the prior example. Since the PSO trajectories are terminated at the desired final velocity, a 3000 m altitude penalty buffer was constructed such that only trajectories that have a terminal altitude error greater than 3000 m are penalized. The resulting optimal PSO solution is shown in Figure 5. As expected, the PSO optimizes to the augmented objective function, and the resulting minimum heat load trajectory terminates at the lowest

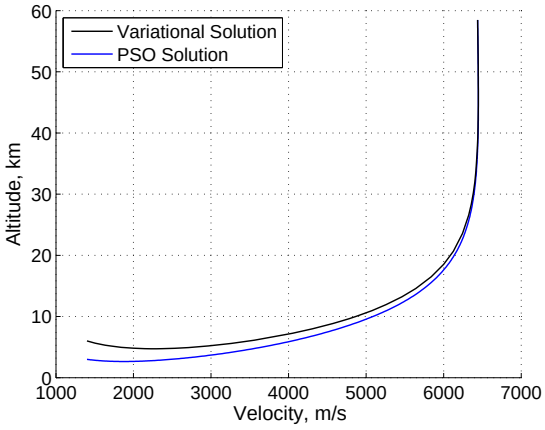

Figure 5. Comparison between variational method and PSO with 3000 m penalty buffer.

altitude within the penalty buffer.

The heat load of this trajectory is only 93% of the heat load associated with the variational solution, and this is accomplished by eliminating the additional heat load incurred when the final altitude is increased. In order to guide the terminal altitude to the desired value, the altitude penalty buffer can be reduced. Figure 6 shows the optimal PSO trajectory when the altitude penalty buffer is reduced to 200 m. As expected, the PSO optimizes to the augmented objective function, and the terminal altitude resides at the lowest altitude within the penalty buffer as shown in Figure 7. By placing a greater emphasis on the terminal conditions, the heat load for this trajectory is 1.09 times greater than that of the variational solution. Furthermore, the time required to construct the PSO solutions is greater than the time required to construct the variational solutions by approximately a factor of eight to ten. This performance gap would also likely be widened if multiple shooting techniques are used to identify the variational solutions.[27]

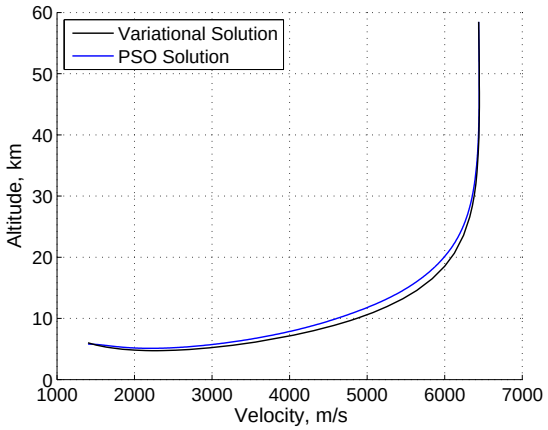

Figure 6. Comparison between variational method and PSO with 200 m penalty buffer.

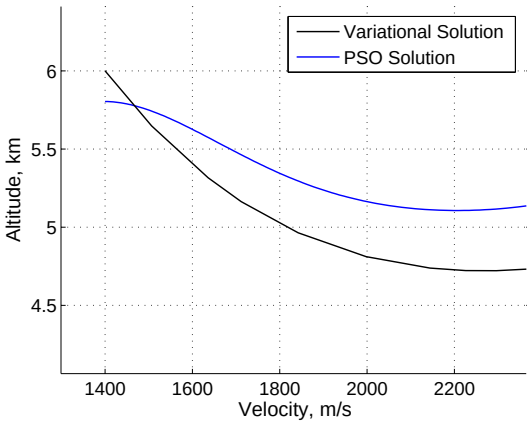

Figure 7. Comparison of terminal trajectory segment with 200 m penalty buffer.

To verify the optimization process, the design space was dramatically reduced to determine if the PSO could arrive to the same solution as that of the variational method. As such, the cone half angle was restricted to $80^o \leq d \leq 90^o$, the initial flight path angle was restricted to $-30^o \leq \gamma_o \leq -10^o$, and the bank angle was restricted to $170^o \leq \phi \leq 180^o$. These ranges were constructed to encompass the variational solution, and the resulting optimal PSO trajectory is shown in Figure 8. As expected, the PSO solution matches the variational solution with a heat load that is only 1% greater than that of the variational solution. This illustrates that the PSO is capable of achieving the same results as the variational method in the prior examples if additional computational resources are provided. Due to the relatively substantial computational resources already required by the PSO, this increase would only further contribute to the computational inefficiency of the approach. As shown, the balance between penalty functions and the original objective adds complexity to the optimization process. While the PSO allows a global search of the design space, the resulting optimal solutions will likely capitalize on the designer's choice of penalty functions. To address this issue, a multi-objective optimization process is constructed that is more robust to the choice in penalty functions.

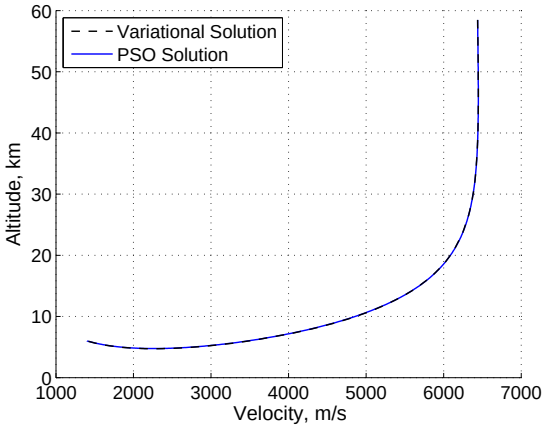

Figure 8. Comparison between variational method and PSO with reduced design space.

To capture optimal solutions that have terminal altitudes closer to the desired value, a second objective in final altitude error is added. As such, a multi-objective particle swarm optimizer (MOPSO) is used to construct the optimal trade, or Pareto frontier, in these two objectives as shown in Figure 9. In this example, the terminal altitude buffer was expanded to 6000 m. During the optimization process, MOPSO attempts

to construct the global Pareto frontier with well-spaced solutions that expand to both ends of the frontier. As expected, the Pareto frontier consists of altitude errors between 0 m and 6000 m. For comparison, a Pareto frontier is also constructed from continuation of variational methods in which the terminal altitude is varied. This process only requires about one-tenth of the computational time when compared to MOPSO. As shown, a well-defined Pareto frontier is constructed using variational methods, and this frontier dominates the MOPSO Pareto frontier. Additionally, the increase in heat load associated with the increase in terminal altitude further validates the single objective PSO trajectories that terminate at the lowest altitude within the penalty buffer. The corresponding MOPSO trajectories are shown in Figure 10 along with a few variational solutions that span the 6000 m altitude penalty buffer. In general, the MOPSO trajectories are consistent with the variational solutions except for a few high-altitude MOPSO trajectories.

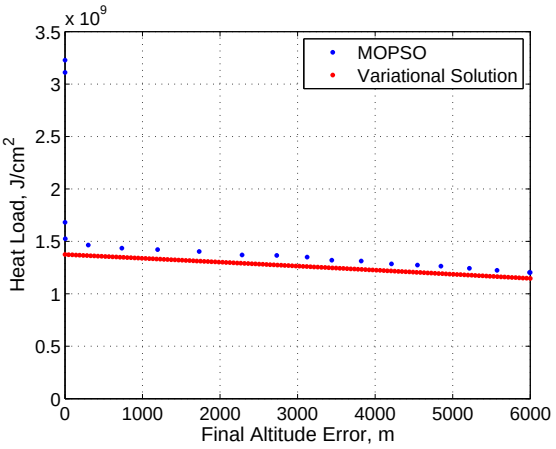

Figure 9. Comparison between variational method and MOPSO frontiers with 6000 m penalty buffer.

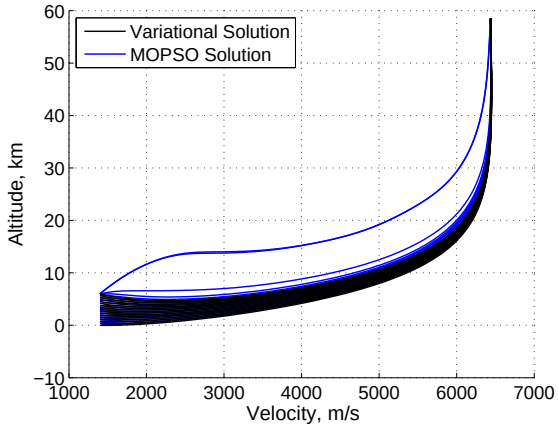

Figure 10. Comparison between variational method and MOPSO trajectories with 6000 m penalty buffer.

These high-altitude trajectories illustrate the difficulty of precisely targeting the desired final altitude when using MOPSO, and these trajectories correspond to the high heat load solutions that have a near zero terminal altitude error shown in Figure 9. While the MOPSO Pareto frontier provides a comprehensive set of optimal solutions, this trade is of little interest to the designer if a terminal altitude error near zero is required. As such, the designer is likely only interested in the design point with a small terminal altitude error near the bend in the frontier. Furthermore, this single design point is obtained by increasing the complexity of the design problem through the addition of a second objective. These examples illustrate the challenges associated with using direct, population-based optimization algorithms commonly used in hypersonic design studies as well as validate the solutions obtained through continuation of variational methods. While the optimal blunted cones minimize heat load, the disk-like shape resulting from a cone half-angle of 90^o is not practical for payload packaging. As such, the trajectory objective must be expanded to include vehicle objectives, such as usable payload volume.

IV.B. Minimum Heat Load and Maximum Usable Volume for a Blended Wedge Subject to Terminal Constraints

To illustrate the diversity of entry vehicle shapes that can be rapidly optimized using the analytic aerodynamic relations, a blended wedge is constructed by combining the aerodynamics of a cylindrical nose, two flat plates, and two half-cones.[8,28] Tangency is enforced among all components of the blended wedge, and the bluntness of the vehicle can be varied through the wedge half angle, d. In this example, the minimum heat load trajectory objective is expanded to also include usable volume in the form shown in Eq. (11), and the Pareto frontier is constructed through continuation of w as shown in Eq. 12. The continuation process begins with $w = 0$ such that the vehicle and trajectory is simultaneously designed to only minimize heat load. During the continuation process, w is incrementally increased to place greater emphasis on usable volume at the penalty of increased heat load. The usable volume of the blended wedge is assumed to reside between the two square-shaped plates that form the upper and lower surfaces of the vehicle. This process only requires about one-tenth of the computational time when compared to MOPSO which was also used to

construct Pareto frontiers of minimum heat load and maximum usable volume.

$$J' = w(-V_{\text{usable}}) + (1-w)\int_{t_0}^{t_f} \dot{q}dt \tag{12}$$

Initially, the design space is chosen to be as large as possible with the wedge half angle restricted to $12^o \leq d \leq 90^o$, the initial flight path angle restricted to $-90^o \leq \gamma_o \leq 0^o$, and the bank angle restricted to $0^o \leq \phi \leq 180^o$. A wedge half angle of 12^o is chosen as a lower bound to provide a reasonable amount of vehicle bluntness based on an assumed set of dimensions. In general, this design space allows MOPSO to explore a wide range of design options when constructing the frontier. Additionally, a third objective in terminal altitude error was included in MOPSO to allow a range of solutions to be constructed within a 200 m terminal altitude buffer. Figure 11 shows the Pareto frontiers constructed using both variational methods and MOPSO, where three times as many iterations were used than the prior MOPSO example. This equates to approximately 25-30 times the computational requirements of the variational method. As shown in Figure 11, many solutions on the MOPSO frontier are heavily dominated by solutions from the variational method. This illustrates a lack of convergence of the MOPSO frontier, even when substantial resources are used. The corresponding trajectories are shown in Figure 12 in which several extreme MOPSO solutions are observed. For example, the MOPSO Pareto frontier points with a usable volume of approximately 0.35-0.45 m^3 that are near the variational solutions correspond to relatively slender vehicles with steep entry flight path angles that terminate at the ground at a velocity of approximately 6500 m/s. These solutions illustrate that the penalty in heat rate for trajectories that terminate outside of the 200 m terminal altitude buffer was not sufficiently strong. Alternatively, the large skipping trajectories illustrate that solutions with accurate terminal conditions remain on the Pareto frontier at a large expense in heat load. These solutions are the result of penalty conditions that are too strong.

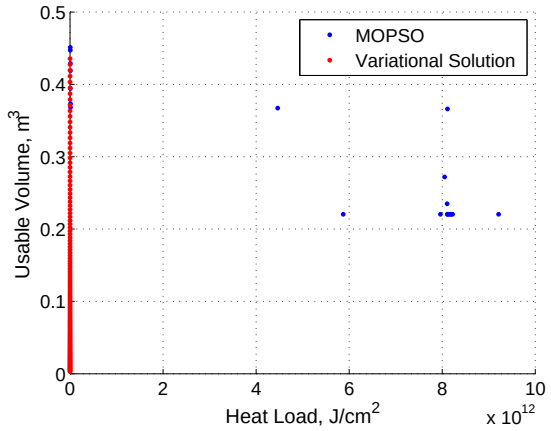

Figure 11. Poor Pareto frontier resulting from large MOPSO design space.

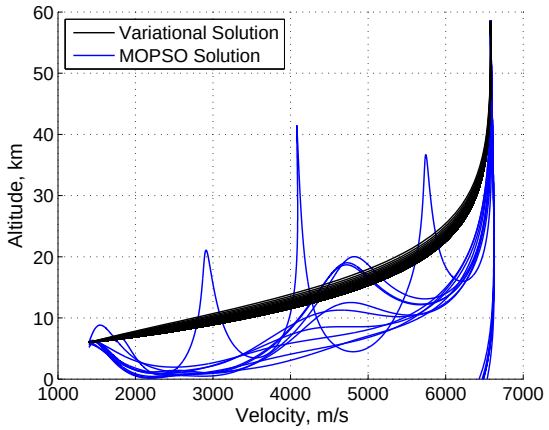

Figure 12. Corresponding trajectory solutions resulting from large MOPSO design space.

To assist MOPSO, the design space was reduced to encompass the Pareto optimal solutions obtained from the variational methods. The smaller design space consists of a wedge half angle restricted to $40^o \leq d \leq 90^o$, an initial flight path angle restricted to $-60^o \leq \gamma_o \leq 0^o$, and a bank angle restricted to $0^o \leq \phi \leq 180^o$. Using the same number of iterations as before, the new MOPSO Pareto frontier is constructed as shown in Figure 13. While the Pareto frontier is dramatically improved, the MOPSO solutions are still dominated by the variational solutions. Additionally, the variational Pareto frontier is more expansive in usable volume than the MOPSO frontier. Note that in both MOPSO frontiers shown in Figures 11 and 13, certain MOPSO solutions appear to be dominated by other MOPSO solutions. This is the result of the third objective in terminal error used to span solutions throughout the 200 m terminal altitude buffer. While this objective is not shown, all MOPSO solutions were verified to reside in this buffer. The corresponding trajectories are shown in Figure 14. While these trajectories have a greater resemblance to the variational solutions, it is clear that certain lofted trajectories with accurate terminal conditions reside on the Pareto frontier at the expense of increased heat loads.

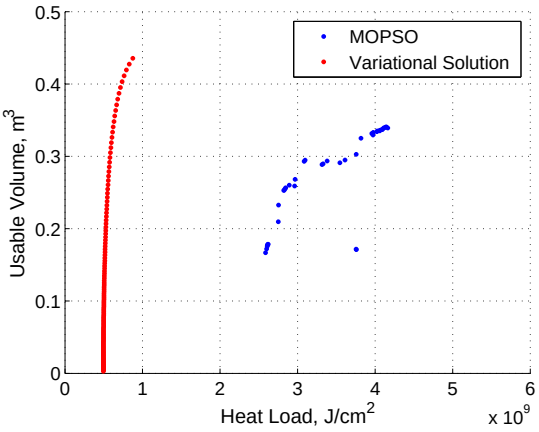

Figure 13. 2-D view of Pareto frontier in volume vs. heat load for blended wedge.

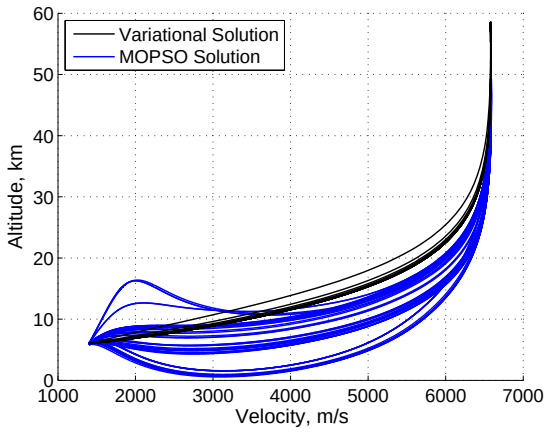

Figure 14. Corresponding trajectories from Pareto frontier.

The evolution of the blended wedge upper surface across the variational Pareto frontier is shown in Figure 15. Analogous to the disk shape of the minimum heat load blunted cone, the minimum heat load blended wedge has the lowest ballistic coefficient. At an angle of attack, this corresponds to a wedge half angle near 90^o, resulting in a geometry with no usable volume. Through continuation of the relative weighting between heat load and usable volume, greater usable volumes are achieved at the expense of higher heat loads that result from increased ballistic coefficients. The cross-section of the nose region shown in Figure 16 illustrates the tangency that is enforced between the flat upper surface and cylindrical nose. As the wedge half angle is decreased, greater portions of the cylindrical nose are exposed, and the altered aerodynamics that result are automatically captured in the analytic aerodynamic relations. As optimal trajectories and vehicle shapes are constructed during the continuation process, these solutions can be monitored to identify limits in vehicle capability. In this example, if the vehicle is made more slender than what is shown, then the vehicle is unable to reach the terminal constraint without flying lofted and eventually skipping trajectories that were chosen to be avoided in this work. This monitoring allows the designer to quickly guide the continuation process to solutions that are of most interest. Note that by using the weighted sum approach from Section III.A.2, the Pareto frontier will only be fully constructed through continuation if the frontier is convex. In both the blunted cone and blended wedge examples, the Pareto frontiers are convex. However, if a more challenging, constrained trajectory is required, then convexity may not be guaranteed. In the following biconic example, the Pareto frontier is non-convex, requiring continuation of a constrained objective.

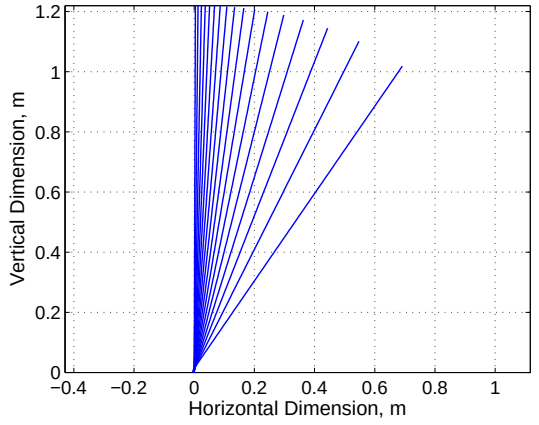

Figure 15. Evolution of blended wedge upper surface cross-section from Pareto frontier.

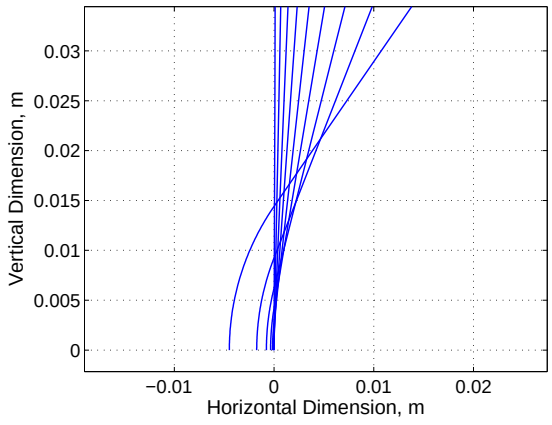

Figure 16. Evolution of blended wedge nose region cross-section from Pareto frontier.

IV.C. Minimum Heat Load and Minimum Required Volume for a Blunted Biconic Subject to Path and Terminal Constraints

The prior example illustrates the ability to construct Pareto frontiers using variational methods when vehicle objectives are included in the optimization. While this example includes terminal constraints, it does not include common path constraints such as maximum heat rate and g-loading. In the following example, a maximum heat rate constraint of approximately 2.0e7 W/cm^2 and a maximum g-loading constraint of approximately 24 Earth-g are chosen. These constraints limit low altitude and high velocity combinations, and prior work has shown that optimal trajectories can be constructed for a fixed vehicle by incrementally introducing these path constraints.[20] This initial continuation process was repeated for a fixed biconic with minor blunting, and this solution serves as a starting point when constructing the Pareto frontier using variational methods. For this example, the vehicle objective is chosen to minimize required volume of the two conical frustums. This objective may result from packaging considerations for storage in a carrier vehicle or launch shroud. Due to concerns of the convexity of the frontier, the required volume is enforced as a constraint, allowing variational methods to be used to optimize the remaining trajectory objective in heat load. The Pareto frontier is then constructed through continuation of the constrained required volume. In order to eliminate the possibility of multiple biconic configurations with the same volume, only the forward conic half angle is allowed to vary to satisfy the volume constraint. Note that this process could also be repeated for the aft conic half angle should these solutions be of interest to the designer.

For comparison, MOPSO was also used to construct the Pareto frontier in which a third objective in terminal altitude error is again introduced. Initially, MOPSO is executed for 300 iterations. Trajectories that violated the heat rate and g-loading constraints were severely penalized to prevent these solutions from appearing in the Pareto frontier. The resulting Pareto frontiers from both MOPSO and the variational method are shown in Figure 17, and the corresponding trajectories are shown in Figure 18. Consistent with the prior examples, the solutions from MOPSO are dominated by solutions constructed from the variational method. While the variational trajectories are tightly grouped together early in the entry, these trajectories form a large band in the second half of the entry. This band is due to the constant g-loading constraint enforced for all optimal solutions. As the forward cone angle is increased to satisfy an increasing required volume constraint during the continuation process, the ballistic coefficient of the vehicle is reduced. As a result, the vehicle must travel at higher altitudes to satisfy the g-loading constraint. While a reduction in ballistic coefficient generally results in shorter flight times that reduce heat load, the higher altitudes that must be flown in the presence of a g-loading constraint increase flight times that also increase heat load. This results in a slightly non-convex Pareto frontier as shown by the variational solutions in Figure 17. Note that the MOPSO solutions that appear to be dominated by other MOPSO solutions are again the result of the third objective in terminal error used to span solutions throughout the 200 m terminal altitude buffer. As such, solutions with much higher heat loads have much smaller terminal errors, and some of the MOPSO solutions close to the variational frontier capitalize on the penalty-free 200 m altitude buffer.

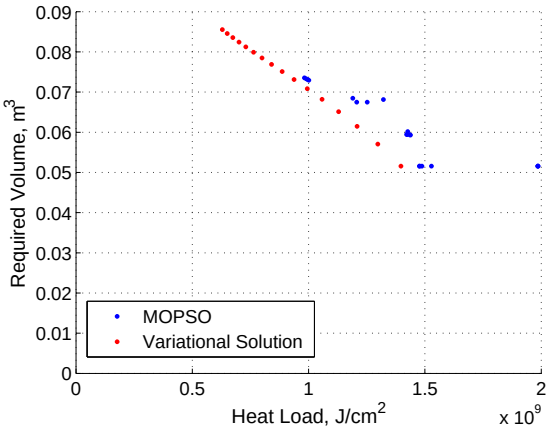

Figure 17. 2-D view of Pareto frontier in required volume vs. heat load for blunted biconic (300 iterations).

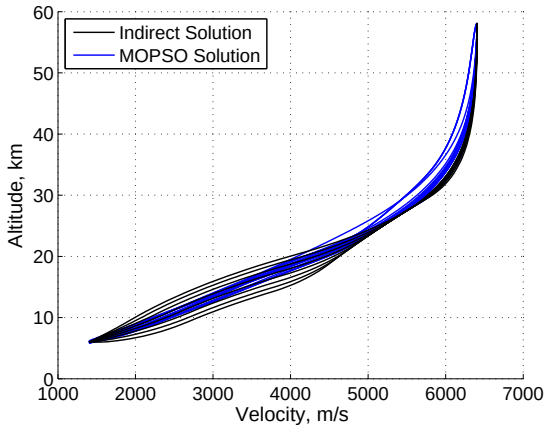

Figure 18. Corresponding trajectories from Pareto frontier (300 iterations).

The MOPSO Pareto frontier shown in Figure 17 has solutions that are grouped together, resulting in a poorly defined frontier. As such, MOPSO is executed for 900 iterations to improve the structure of the frontier, requiring approximately 25-30 times the computational requirements of variational methods. As shown in Figure 19, the new MOPSO Pareto frontier is better distributed with many solutions near the variational frontier. Additionally, the corresponding MOPSO trajectories shown in Figure 20 also have an increased distribution where the g-loading constraint is active along the second half of the trajectory. However, a select number of high-altitude trajectories are introduced. These trajectories correspond to slender biconic solutions that have small terminal altitude errors. This result is largely due to the difficulty of constructing path-constrained optimal trajectories using direct shooting methods. To follow the g-loading constraint, the vehicle must dive further into the atmosphere near a velocity of 4500 m/s. Complex maneuvers such as these are difficult to construct when using direct shooting methods. The evolution of the blunted biconic shape is shown for three optimal solutions in Figure 21. Note that as the forward cone angle is increased, greater portions of the aft conic is exposed, and the resulting change in aerodynamics is automatically captured through the use of analytic hypersonic aerodynamic relations.

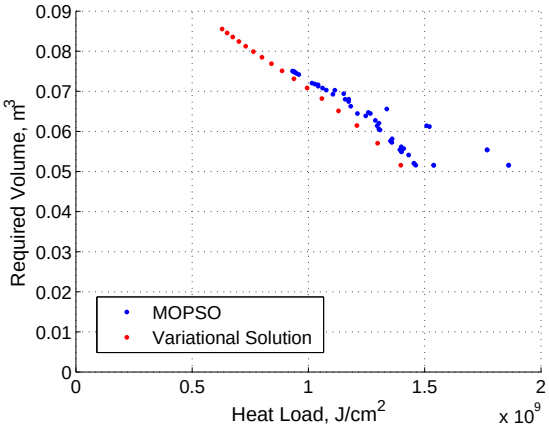

Figure 19. 2-D view of Pareto frontier in required volume vs. heat load for blunted biconic (900 iterations).

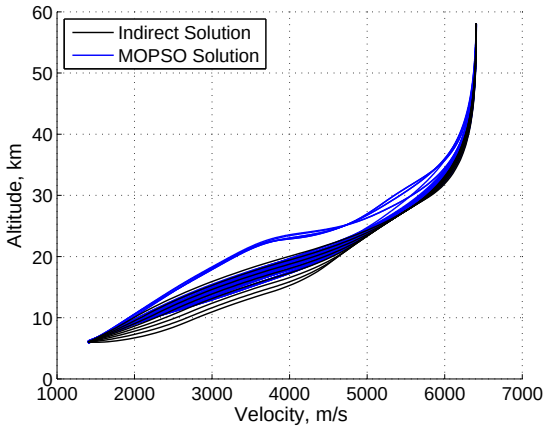

Figure 20. Corresponding trajectories from Pareto frontier (900 iterations).

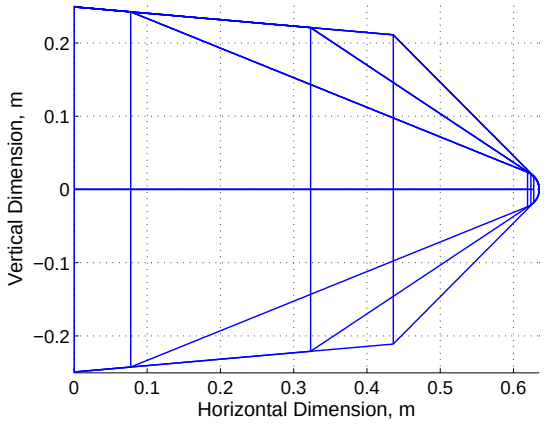

Figure 21. Samples from evolution of blunted biconic geometry.

V. Future Work

When using variational methods, certain costate equations require derivatives of the analytic aerodynamic relations with respect to vehicle shape parameters. While the analytic expressions are reasonable in length for the geometries in this report, their lengthy derivative expressions can result in compiling issues during the autocoding process. These issues are eliminated by reducing the length of the derivative expressions through variable substitution of repetitive calculations. As a result, each repetitive calculation is evaluated only once. Furthermore, these substitutions improve code efficiency, resulting in a reduction in computational requirements by a factor of two to four. Additional advancement in code optimization could provide a further reduction in computational requirements as well as enable more complex geometries, such as Bezier curves of revolution, to be incorporated into the variational methodology.[8] This could be accomplished through further investigation in symbolic and string manipulation techniques or other computational techniques such as automatic differentiation.[29,30] If the analytic aerodynamics are constructed for potential adaptive shapes, such as inflatable aerodynamic decelerators, then the optimization in this work could be extended to include

vehicle shape change during flight.

This work illustrates the benefit of using variational methods with analytic aerodynamic force coefficients to address trajectory performance. If analytic aerodynamic moment coefficients are also included, then additional considerations such as aerodynamic stability and control surface design could be included in the optimization process.[8] Furthermore, other disciplines in the DSM shown in Figure 1 should also be evaluated for incorporation into this rapid design methodology. Analogous to the analytic hypersonic aerodynamics, physics-based models associated with these other disciplines should be investigated. If useful physics-based models are not available, then analytic metamodels could be constructed as a substitute. Finally, more efficient variational solution solvers such as BNDSCO should be evaluated to determine if additional performance enhancements can be achieved.[27]

VI. Conclusions

In this investigation, a rapid simultaneous hypersonic aerodynamic and trajectory optimization methodology is constructed based on variational methods. This design framework is made possible from enabling advancements in analytic hypersonic aerodynamics and rapid trajectory optimization that relies on continuation of variational methods. By extending this rapid trajectory optimization methodology to include the analytic aerodynamic relations, an augmented system is constructed that includes both trajectory and vehicle shape parameters. A single and multi-objective particle swarm optimizer is used as a representative state-of-the-art multidisciplinary optimization methodology that relies on direct shooting for trajectory optimization. Comparisons illustrate that improved solutions can be obtained through continuation of variational methods. Furthermore, variational methods are shown to be effective across a range of vehicle shapes that include blunted cones, blended wedges, and blunted biconics for single and multiple design objectives in trajectory and vehicle shape. For the examples shown, the computational requirements for the particle swarm optimizer are approximately 10-30 times greater than that of the variational methods.

Examples also demonstrate the challenges of using penalty functions with direct shooting methods when trajectory constraints are present. If penalty functions are too strong, then the design objective is ignored during the optimization. If the penalty functions are too weak, then the optimizer will capitalize on the ability to construct improved solutions that violate the constraints. If the constraint is converted into an additional objective, then a multi-objective particle swarm optimizer is able to construct solutions near the constraint at the expense of increased complexity resulting from the additional objective. Variational methods are shown to be able to perform the constrained optimization across a wide range of designs by precisely satisfying constraints without the added complexity of penalty functions. For convex Pareto frontiers, this optimization is most efficiently performed through continuation of a weighted sum of the individual objectives. Finally, a non-convex frontier is shown to be easily constructed through continuation of a constrained objective.

References

[1]Acton, D. E. and Olds, J. R., "Computational Frameworks for Collaborative Multidisciplinary Design of Complex Systems," AIAA 98-4942, *7th AIAA/USAF/NASA/ISSMO Symposium on Multidisciplinary Analysis and Optimization*, St. Louis, MO, 2-4 Sep. 1998.

[2]Olds, J. R., "The Suitability of Selected Multidisciplinary Design and Optimization Techniques to Conceptual Aerospace Vehicle Design," AIAA 92-4791, *4th AIAA/USAF/NASA/OAI Symposium on Multidisciplinary Analysis and Optimization*, Cleveland, OH, 21-23 Sep. 1992.

[3]Braun, R. D., Powell, R. W., Lepsch, R. A., Stanley, D. O., and Kroo, I. M., "Comparison of Two Multidisciplinary Optimization Strategies for Launch-Vehicle Design," *Journal of Spacecraft and Rockets*, Vol. 32, No. 3, 1995.

[4]Brown, N. F. and Olds, J. R., "Evaluation of Multidisciplinary Optimization Techniques Applied to a Reusable Launch Vehicle," *Journal of Spacecraft and Rockets*, Vol. 43, No. 6, 2006.

[5]Perez, R. E., Liu, H. H. T., and Behdinan, K., "Evaluation of Multidisciplinary Optimization Approaches for Aircraft Conceptual Design," AIAA 2004-4537, *10th AIAA/ISSMO Multidisciplinary Analysis and Optimization Conference*, Albany, NY, 30 Aug. - 1 Sep. 2004.

[6]Steinfeldt, B., Theisinger, J., Korzun, A., Clark, I., Grant, M., and Braun, R., "High Mass Mars Entry Descent and Landing Architecture Assessment," AIAA 2009-6684, *AIAA Space 2009*, Pasadena, CA, 14 - 17 Sept. 2009.

[7]Garcia, J. A., Brown, J. L., Kinney, D. J., Bowles, J. V., Huynh, L. C., Jiang, X. J., Lau, E., and Dupzyk, I. C., "Co-Optimization of Mid Lift to Drag Vehicle Concepts for Mars Atmospheric Entry," AIAA 2010-5052, *10th AIAA/ASME Joint Thermophysics and Heat Transfer Conference*, Chicago, IL, 28 Jun. - 1 Jul. 2010.

[8]Grant, M. J. and Braun, R. D., "Analytic Hypersonic Aerodynamics for Conceptual Design of Entry Vehicles," AIAA 2010-1212, *48th AIAA Aerospace Sciences Meeting Including the New Horizons Forum and Aerospace Exposition*, Orlando, FL, 4-7 Jan. 2010.

[9]Grant, M. J., Clark, I. G., and Braun, R. D., "Rapid Entry Corridor Trajectory Optimization for Conceptual Design," AIAA 2010-7810, *AIAA Atmospheric Flight Mechanics Conference and Exhibit*, Toronto, Ontario, Canada, 2-5 Aug. 2010.

[10]Otero, R. E. and Braun, R. D., "The Planetary Entry Systems Synthesis Tool: A Conceptual Design and Analysis Tool for EDL Systems," IEEEAC 1331, *2010 IEEE Aerospace Conference*, Big Sky, MT, Mar. 2010.

[11]Anderson, J. D., *Hypersonic and High Temperature Gas Dynamics*, AIAA, 1989.

[12]Bonner, E., Clever, W., and Dunn, K., "Aerodynamic Preliminary Analysis System II: Part I Theory," *NASA-CR-165627*, Apr. 1981.

[13]Smyth, D. N. and Loo, H. C., "Analysis of Static Pressure Data from 1/12-scale Model of the YF-12A. Volume 3: The MARK IVS Supersonic-Hypersonic Arbitrary Body Program, User's Manual," *NASA-CR-151940*, Oct. 1981.

[14]Cunningham, M., "Hypersonic Aerodynamics for an Entry Research Vehicle," *Journal of Spacecraft and Rockets*, Vol. 24, No. 2, 1987.

[15]Kinney, D. J., "Aero-Thermodynamics for Conceptual Design," AIAA-2004-31-962, *42nd AIAA Aerospace Sciences Meeting and Exhibit*, Reno, NV, 5-8 Jan. 2004.

[16]Kirk, D. E., *Optimal Control Theory: An Introduction*, Prentice-Hall, Inc., 1970.

[17]McCausland, I., *Introduction to Optimal Control Theory*, John Wiley and Sons, Inc., 1969.

[18]Bryson, A. E. and Ho, Y.-C., *Applied Optimal Control*, Taylor and Francis, 1975.

[19]Elsgloc, L. D., *Calculus of Variations*, Dover Publications, Inc., 2007.

[20]Grant, M. J., Clark, I. G., and Braun, R. D., "Rapid Design Space Exploration for Conceptual Design of Hypersonic Missions," *AIAA Atmospheric Flight Mechanics Conference and Exhibit*, Portland, OR, 8-11 Aug. 2011 (to be published).

[21]Messac, A. and Ismail-Yahaya, A., "Required Relationship Between Objective Function and Pareto Frontier Orders: Practical Implications," *AIAA Journal*, Vol. 39, No. 11, 2001.

[22]Messac, A., Sundararaj, G. J., Tappeta, R. V., and Renaud, J. E., "Ability of Objective Functions to Generate Points on Nonconvex Pareto Frontiers," *AIAA Journal*, Vol. 38, No. 6, 2000.

[23]de Weck, O. and Kim, I. Y., "Adaptive Weighted Sum Method for Bi-objective Optimization," AIAA 2004-1680, *45th AIAA/ASME/ASCE/AHS/ASC Structures, Structural Dynamics and Materials Conference*, Palm Springs, CA, 19-22 Apr. 2004.

[24]Grant, M. J. and Mendeck, G. F., "Mars Science Laboratory Entry Optimization Using Particle Swarm Methodology," AIAA 2007-6393, *AIAA Atmospheric Flight Mechanics Conference and Exhibit*, Hilton Head, SC, 20-23 Aug. 2007.

[25]Lafleur, J. and Cerimele, C., "Mars Entry Bank Profile Design for Terminal State Optimization," AIAA 2008-6213, *AIAA Atmospheric Flight Mechanics Conference and Exhibit*, Honolulu, HI, 18-21 Aug. 2008.

[26]Wolpert, D. H. and Macready, W. G., "No Free Lunch Theorems for Optimization," *Technical Report, IBM Almaden Research Center and Santa Fe Institute*, 1996.

[27]Oberle, H. J. and Grimm, W., BNDSCO: A Program for the Numerical Solution of Optimal Control Problems, University of Hamburg, Hamburg, Germany, Oct. 2001.

[28]Kinney, D. J. and Bowles, J. V., "Conceptual Design of a 'SHARP'-CTV," AIAA 2001-2887, *35th AIAA Thermophysics Conference*, Anaheim, CA, 11-14 Jun. 2001.

[29]Su, J. and Renaud, J. E., "Automatic Differentiation in Robust Optimization," *AIAA Journal*, Vol. 35, No. 6, 1997.

[30]Turner, J. D., "Automated Generation of High-Order Partial Derivative Models," *AIAA Journal*, Vol. 41, No. 8, 2003.